

Confinement-Induced versus Correlation-Induced Electron Localization and Wave Function Entanglement in Semiconductor Nano Dumbbells

A. Franceschetti,^{*,†} L. W. Wang,[‡] G. Bester,[†] and A. Zunger[†]

National Renewable Energy Laboratory, Golden, Colorado 80401, and
Computational Research Division, Lawrence Berkeley National Laboratory,
Berkeley, California 94720

Received December 20, 2005; Revised Manuscript Received March 7, 2006

ABSTRACT

Single-particle plus many-particle calculations of the electronic states of semiconductor nano dumbbells show how geometrical features (e.g., the width of the dumbbell wire) determine, through quantum confinement and electron–electron correlation effects, the spatial localization and the degree of entanglement of the electronic wave functions. Remarkably, we find that correlation effects can alter carrier localization and that the degree of wave function entanglement can be tuned by changing the diameter of the dumbbell wire. We further show how the exciton binding energy depends on the nano dumbbell geometry.

The current technological pursuit of electronic nanodevices,^{1–6} based on two-dimensional (2D) quantum wells, one-dimensional (1D) quantum wires, and zero-dimensional (0D) quantum dots of ever decreasing sizes, is rapidly approaching systems where carrier localization and transport are entirely controlled by quantum effects. Transistors made of a carbon nanotube,¹ or a single semiconductor nanowire,² or a few colloidal nanocrystals,³ as well as single electron^{4,5} or hole⁶ tunneling devices, all exemplify the trend toward low dimensionality, nanometer-sized circuit components, as envisioned by the electronic industry road map.⁷ Recently, nanosystems consisting of coupled quantum dots (quantum dot molecules) have been proposed as a basis for quantum computing,⁸ triggering fervent activity in this field. In the original scheme,⁸ the electrons localized in the dots represent the qubits, and spin–spin interactions between them determine the time evolution of the coupled system. Systems consisting of quantum dots connected by quantum wires offer several degrees of freedom (dot size, wire length, wire diameter, etc.) that can be tuned to optimize the degree of carrier localization and wave function entanglement toward nanodevice and quantum-computing applications.

Most theoretical descriptions of nanosystems pertain to isolated building blocks, such as 0D quantum dots,⁹ 1D

quantum wires,¹⁰ and 2D quantum wells,¹¹ and little is known on the quantum behavior of complex assemblies of such building blocks. Recent calculations for “dot molecules”¹² and “dot crystals”¹³ have already revealed the importance of potentially transport-impeding effects, such as correlation-induced (Mott) localization of the carriers on fragments (building blocks) of the entire system. Of particular interest here are such quantum effects in complex nanostructures, consisting of an assembly of building blocks of different shape and dimensionality. Consider, for example, a “nano dumbbell” made of two dots of radius R_D connected by a quantum wire of radius R_W . Such systems have been recently made, e.g., by Mokari et al.¹⁴ Figure 1 illustrates how the single-particle electronic structure could depend critically on the wire radius R_W . For a wide wire (Figure 1a), reduced quantum confinement in the wire causes the wire electron energy level e_W to drop below the dot energy levels e_D , with ensuing localization of the electron wave function on the 1D wire segment. For a narrow wire (Figure 1b), increased quantum confinement in the wire raises the energy level e_W above e_D , leading to migration of the electron wave function into the 0D dots. It is likely, however, that many-particle effects could modify this picture in a substantial way. Consider, for example, the case of two electrons simultaneously present in the dumbbell system. Electron correlation induced by the energetic and spatial proximity of various single-particle states (Figure 1) would lead to a mixture of

* Author to whom correspondence should be addressed. E-mail: alberto_franceschetti@nrel.gov.

[†] National Renewable Energy Laboratory.

[‡] Lawrence Berkeley National Laboratory.

Nano – Dumbbells: Expectations

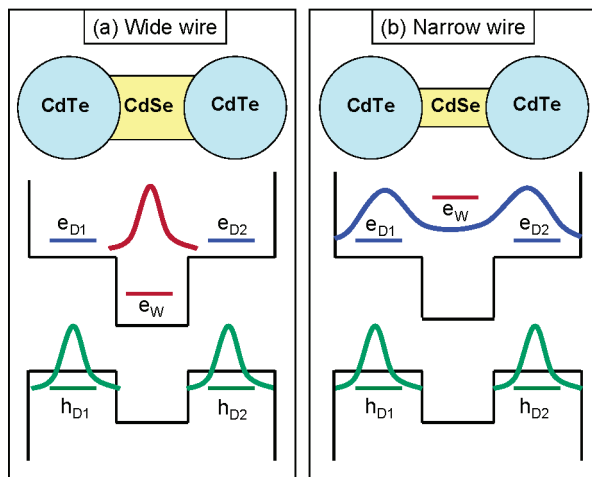


Figure 1. Schematic diagram of the energy levels and wave functions of (a) wide-wire and (b) narrow-wire nano dumbbells, where coupling between the dots and the wire is neglected. The black solid lines show the conduction-band and valence-band offsets of bulk CdTe and CdSe. The levels h_{D1} and h_{D2} are the VBM states of the two dots. The levels e_{D1} , e_{D2} , and e_W are the CBM states of the dots and the wire, respectively. In the case of a wide wire (a), the VBM wave function is localized on the dots, while the CBM wave function is localized on the wire. In the opposite case of a narrow wire (b), both the VBM and the CBM are localized on the dots.

the single-particle ground and excited states. Depending on the relative sizes R_D and R_W , the many-particle wave function (made of a coherent superposition of single-particle states) could be delocalized over the entire wire + dots system, even though the lowest-energy single-particle states are localized only on the wire or on the dots.

Although the nano dumbbell is a closed system, it is interesting to consider how it will behave electronically under transport conditions. Depending on the kinetics of carrier injection, the system can contain either one or several electrons.¹⁵ The spatial localization of the electrons is controlled by quantum confinement and correlation effects. For example, if the nano dumbbell contains two electrons, then for a narrow wire the natural propensity will be for each dot to contain one electron, whereas for a wide wire both electrons will be in the wire. External bias, under transport conditions, will have to overcome such energetic preferences that are induced by many-particle effects. Yet, the spatial distribution of carriers is often described theoretically via one-particle effects alone. What we propose here is a general approach that describes quantitatively the balance between one-electron and many-electron effects and can accurately predict the degree of carrier localization and wave function entanglement in complex nanostructures. The only input to the calculation is the composition, shape, and size of the nanostructures. Thus, if those are determined experimentally for a series of nanostructures, then we can identify which will be dominated by single-particle effects and which will be dominated by correlation effects.

Several methodologies are available in the literature for combining a single-particle description with a many-body

treatment. “First-generation” approaches are based on continuum effective-mass single-particle theories, such as the one-band particle-in-a-box effective-mass approximation (see, e.g., ref 16) or the few-band \mathbf{k}, \mathbf{p} approximation (e.g., ref 17). These continuum-like effective-mass approaches have been combined with many-body treatments such as quantum Monte Carlo¹⁸ or configuration interaction (either for \mathbf{k}, \mathbf{p} ¹⁹ or for the single-band effective mass²⁰), enabling calculations of large (up to 10^7 atoms) systems. These single-particle approaches model quantum confinement but either neglect¹⁶ or oversimplify¹⁷ the effects of interband coupling (i.e., the coupling between various bands at a given point of the Brillouin zone), intervalley coupling (e.g., the coupling between the Γ , X, and L valleys), and strain. These approximations lead to quantitative²¹—and often even qualitative²²—errors in the single-particle energies and wave functions. For example, simple effective-mass models do not include heavy hole/light hole mixing, which is primarily responsible for the bonding–antibonding splitting of the hole states in dot molecules.²³ “Second generation” approaches are based on atomistic single-particle theories (such as tight-binding²⁴ or empirical pseudopotentials²⁵), which include a broad range of single-particle effects (e.g., interband and intervalley coupling, strain, compositional inhomogeneity), albeit via empirical parametrization of the bulk Hamiltonian. These approaches have also been combined with many-body approaches, such as configuration interaction (either in the context of tight-binding²⁶ or pseudopotentials²⁷), enabling calculations on 10^3 – 10^6 atom systems. What we are aiming at is a “third-generation” approach, based on first-principles atomistic single-particle theories, such as density-functional theory in the local-density approximation (LDA), combined with a sophisticated many-body approach. To date, such combinations of methodologies are limited to tiny nanostructures,^{28,29} because both the single-particle LDA method and the many-body approaches are enormously demanding from a computational point of view. Here we combine an atomistic, LDA-quality single-particle “charge-patching” approach³⁰ with a configuration-interaction many-particle method²⁷ to calculate quantum confinement and electron localization in semiconductor nano dumbbells containing up to 6000 atoms.

We consider semiconductor nano dumbbells consisting of two nearly spherical CdTe dots of radius $R_D = 25 \text{ \AA}$, connected by a 30- \AA -long CdSe wire of variable radius R_W . CdTe quantum dots are usually grown in the zinc blende lattice structure. Here we assume that the CdSe wire is grown pseudomorphically along the (100) crystallographic orientation and that it inherits the zinc blende lattice structure of the CdTe dots. Surface atoms are passivated using a ligandlike potential,³¹ which acts to remove surface states from the band gap. Figure 2 shows the atomistic structure of one of the nano dumbbells used in the calculations ($R_W = 10 \text{ \AA}$). This system consists of 2268 Cd atoms, 2100 Te atoms, 169 Se atoms, and 1436 passivants, for a total of 5973 atoms. The atomic positions are relaxed using an atomistic valence force field model. The parameters of this model are fitted to the bulk elastic constants of the constituents. The

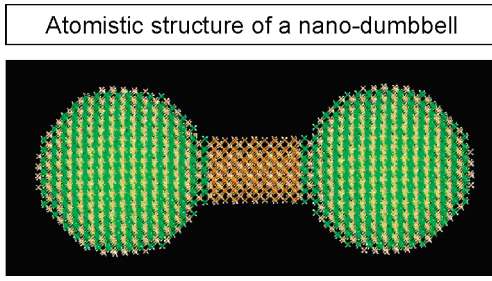


Figure 2. Atomistic positions of a CdTe/CdSe nano dumbbell ($R_W = 10 \text{ \AA}$) containing a total of 5973 atoms.

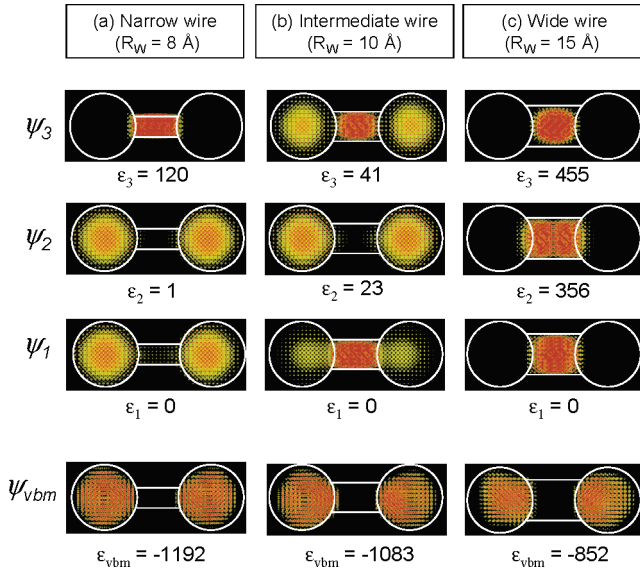


Figure 3. Calculated single-particle energies and wave functions of the three nano dumbbells considered in this work. For each wire size, we show the atomistic wave functions of the topmost valence state (ψ_{VBM}) and the first three conduction-band states (ψ_1 , ψ_2 , and ψ_3). Also shown are the single-particle energies (in meV), measured with respect to the CBM (i.e., $\epsilon_1 = 0$).

total valence charge density of the relaxed system is then constructed using the charge-patching method.³⁰ In this method, small prototype systems with similar local atomic structures as the dumbbell are calculated self-consistently using LDA. The total charge density of these prototype systems is decomposed into charge-density motifs belonging to different atoms. These charge motifs are then assembled to generate the total charge density of the dumbbell. The typical density error generated this way is less than 1% compared to direct LDA calculations.³⁰ After the charge density is obtained, the LDA is used to generate the total electronic potential. The ensuing single-particle Schrodinger equation is then solved using the folded spectrum method²⁵ to calculate band-edge states. The detailed procedure of the charge-patching method was reported in ref 30.

The calculated single-particle wave functions and energies of several band-edge states are shown in Figure 3 for three values of R_W . The localization of the band-edge states can be understood qualitatively by considering the CdSe wire and the two CdTe dots as separate building blocks and allowing perturbative coupling between the single-particle states of the wire (W) and the dots (D_1 and D_2), as illustrated

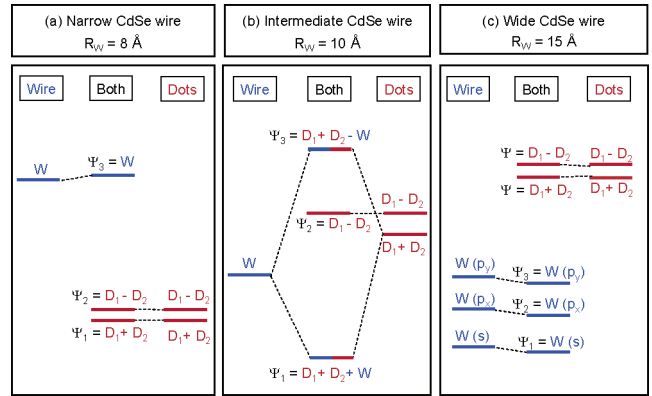


Figure 4. Schematic diagram of the single-particle levels of the isolated building blocks (wire and dots) and of the coupled (wire + dots) system. Wire states are shown in blue, dot states in red.

in Figure 4. For all of the dumbbell geometries considered here, the valence-band maximum (VBM) is an antibonding combination of the two s-like valence states localized on the CdTe dots (bottom panels of Figure 3). This is so because the valence band offset between CdTe and CdSe³² (Figure 1) places the VBM of CdSe deeper in energy. Figure 3 shows that the wave function character of the conduction-band minimum (CBM) depends strongly on the radius R_W of the wire. In the case of a narrow wire (Figures 3a and 4a), quantum confinement pushes the energy of the wire states well above the lowest-energy dot states, and coupling between dot states and wire states is relatively small. As a result, the lowest-energy electron states, ψ_1 and ψ_2 , correspond to bonding and antibonding combinations of pure dot states ($D_1 \pm D_2$), as shown in Figures 3a and 4a. In the opposite case of a wide wire (Figures 3c and 4c), the lowest-energy wire state (W) drops below the dot states ($D_1 \pm D_2$) as a result of reduced quantum confinement. The CBM ψ_1 corresponds to an s-like state localized on the wire (Figures 3c and 4c). The next two states ψ_2 and ψ_3 are also localized on the wire and have p_x - and p_y -like envelope functions, respectively. In the case of a wire of intermediate size (Figures 3b and 4b), we observe strong coupling between wire and dots conduction states. The dot–dot bonding state ($D_1 + D_2$) is strongly coupled to the wire s-like state (W). This coupling leads to a CBM made of the bonding combination $\psi_1 = D_1 + D_2 + W$. Interestingly, the antibonding combination $\psi_3 = D_1 + D_2 - W$ is higher in energy than the dot–dot antibonding state $\psi_2 = D_1 - D_2$, because by symmetry $D_1 - D_2$ cannot couple to wire s-like states.

To examine the effects of electron–electron interactions on the localization of the wave functions, we consider a system of two conduction-band electrons in the dumbbell. The calculation of the many-body states is performed using the configuration-interaction (CI) approach described in ref 27. First, we calculate screened electron–electron Coulomb and exchange integrals of the form

$$J_{ij,kl} = \sum_{\sigma} \int \psi_i^*(r,\sigma) \psi_j(r,\sigma) \Phi_{kl}(r) dr \quad (1)$$

where $\psi_i(r,\sigma)$ are the single-particle wave functions (Figure

3), which depend on the spatial variable r and the spin variable σ , and $\Phi_{ji}(r)$ is the solution of the generalized Poisson equation

$$\nabla\epsilon(r)\nabla\Phi_{ji}(r) = -4\pi \sum_{\sigma} \psi_j^*(r,\sigma)\psi_i(r,\sigma) \quad (2)$$

The Coulomb interaction is screened by the dielectric function $\epsilon(r)$, which has the value $\epsilon_{\text{in}}(r)$ inside the nano dumbbell and decays to ϵ_{out} outside the nano dumbbell. Recent first-principles calculations^{33,34} have shown that $\epsilon_{\text{in}}(r)$ can be approximated by the dielectric constant of the bulk constituents. Semiconductor nanocrystals are often grown in solution, so typical values for ϵ_{out} are between 2 and 5. However, in the case of nano circuits, one expects ϵ_{out} to be affected by the presence of the substrate, metallic electrodes, etc., which tend to increase the value of ϵ_{out} . Given this uncertainty, we have chosen $\epsilon_{\text{out}} = \epsilon_{\text{CdTe}}$. In the next step, we set up and diagonalize the configuration-interaction Hamiltonian using a basis set of Slater determinants (configurations). In all cases considered here, the basis set consists of the orbital and spin configurations constructed from the first three conduction-band states (ψ_1 , ψ_2 , and ψ_3), corresponding to 15 Slater determinants. All other conduction-band states are much higher in energy, so their contribution to low-energy many-particle states is small. Once the many-particle wave functions have been obtained, we calculate the pair correlation function $P_I(r,r') = |\Psi_I(r,r')|^2$, where $\Psi_I(r,r')$ is the two-particle wave function of state I obtained from the CI calculation. $P_I(r,r')$ gives the probability of finding one electron at r given that the second electron is located at r' .³⁵ We also calculate the degree of entanglement (DOE) using a generalization of the Von Neumann definition of entanglement to identical fermions.³⁶

The results of the many-body calculations are shown in Figures 5–7, where, for transparency of the pertinent physics, we consider four levels of approximation (from left to right in each figure): (a) In the single-particle approximation, the energy of the configuration $|\psi_i\psi_j\rangle$ (a single Slater determinant constructed from the single-particle orbitals ψ_i and ψ_j) is given by the sum of the single-particle energies ($\epsilon_i + \epsilon_j$). (b) In the next level of approximation (single-particle plus diagonal Coulomb), we include the diagonal Coulomb energies ($J_{ij,ij}$), describing the direct repulsion between an electron in the single-particle state ψ_i and an electron in ψ_j . This is equivalent to first-order perturbation theory.²⁷ (c) In the “single-configuration” approximation, the Coulomb and exchange interactions between different spin configurations corresponding to the same orbital configuration are included. Thus, each configuration $|\psi_i\psi_j\rangle$ (with $i \neq j$) splits into a singlet and a triplet. (d) Finally, in the full configuration-interaction calculations all of the orbital and spin configurations consistent with a given number of single-particle states are used to expand the many-body wave functions.

In the case of the wide-wire dumbbell the first few conduction states (ψ_1 , ψ_2 , and ψ_3) are all localized on the wire and are separated by large energy spacings (Figure 3c). As a result, correlation effects are small (Figure 5), and the two electrons in the dumbbell form a singlet state $|\psi_1\psi_1\rangle$

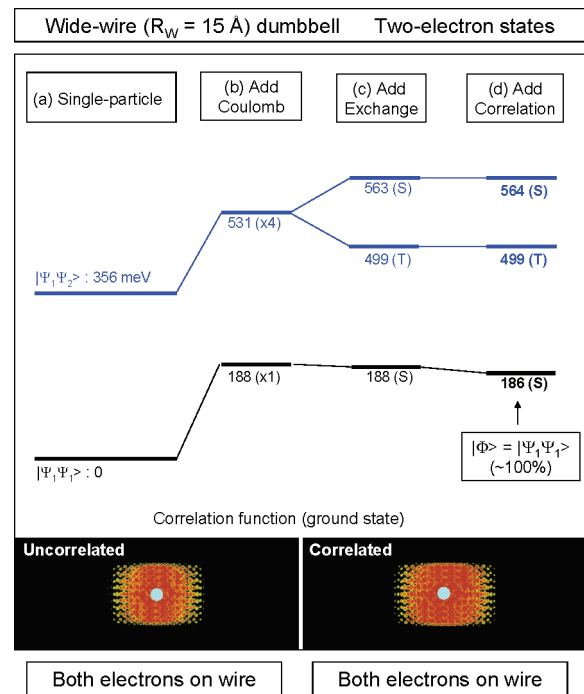


Figure 5. Energy levels (in meV) of two electrons in a wide-wire nano dumbbell ($R_w = 15 \text{ \AA}$). The correlation function in the uncorrelated (single-particle) and correlated (full CI) cases is shown at the bottom of the figure. The correlation function gives the probability of finding one electron in different regions of the dumbbells (yellow cloud), when the other electron is kept fixed at the center of the CdSe wire (blue circle).

corresponding to double occupancy of the lowest-energy wire state ψ_1 . Since the ground state can be described by a single Slater determinant, the DOE is nearly zero. The correlation function (bottom panel of Figure 5) is very similar in the correlated and uncorrelated cases: If one electron (blue circle) is placed at the center of the wire, then the second electron (orange cloud) is also localized on the wire. The excited states are a singlet and a triplet derived from $|\psi_1\psi_2\rangle$, with an exchange splitting of 64 meV.

In the opposite situation of a thin-wire dumbbell (Figure 6), the first two conduction states (ψ_1 and ψ_2) are bonding and antibonding linear combinations of dots states, respectively (Figure 3a). We can construct three configurations of the two-electron system using ψ_1 and ψ_2 : two singly degenerate configurations, $|\psi_1\psi_1\rangle$ and $|\psi_2\psi_2\rangle$, and one 4-fold degenerate configuration $|\psi_1\psi_2\rangle$. These configurations are shifted upward in energy by direct electron–electron Coulomb interaction (Figure 6b). The electron–electron exchange interaction (Figure 6c) splits the configuration $|\psi_1\psi_2\rangle$ into a singlet and a triplet, separated by 110 meV. Finally, correlation effects (Figure 6d) strongly mix the configurations $|\psi_1\psi_1\rangle$ and $|\psi_2\psi_2\rangle$, leading to a many-body singlet ground state that is a linear combination of those two configurations. This state has the maximum possible degree of entanglement (DOE = 100%). Since in the single-particle description the first wire state is significantly higher in energy than the dot states (Figure 3a), the physics of the two-electron dumbbell system is analogous to that of two dots without a connecting wire.³⁵ The first four two-particle states correspond to the two electrons being localized on different dots (with the

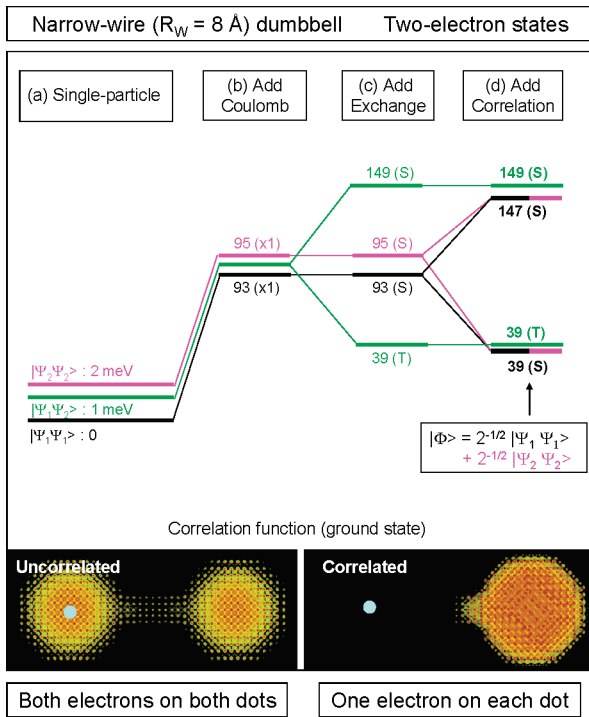


Figure 6. Energy levels (in meV) of two electrons in a narrow-wire nano dumbbell ($R_w = 8 \text{ \AA}$). The correlation function in the uncorrelated (single-particle) and correlated (full CI) cases is shown at the bottom of the figure. The correlation function gives the probability of finding one electron in different regions of the dumbbells (yellow cloud), when the other electron is kept fixed at the center of the left-hand side CdTe dot (blue circle).

singlet state slightly lower in energy than the triplet state), as a result of electron–electron repulsion. The next two states correspond to the two electrons being localized on the same dot. The localization of the electrons on opposite dots is driven by correlation effects, as demonstrated by the correlation function plot shown at the bottom of Figure 6. When one electron is located at the center of the left-hand side dot (blue circle), then the second electron (yellow cloud) is delocalized on both dots in the uncorrelated case, but only on the right-hand side dot in the correlated case.

Finally, we consider the case of intermediate wire thickness (Figure 7). In this case there are several two-electron configurations in a narrow ($<100 \text{ meV}$) energy window (Figure 7a). Direct Coulomb interactions change the order of the configuration energies (Figure 7b). In particular, the configuration $|\psi_1\psi_2\rangle$ is pushed lower in energy than $|\psi_1\psi_1\rangle$, as a result of reduced Coulomb repulsion (83 vs 150 meV). Configurations that are 4-fold degenerate (due to spin degeneracy) at the single-particle level (Figures 7a and 7b) split into a singlet and a triplet in the single-configuration approximation (Figure 7c). The ground state is the triplet state originating from the configuration $|\psi_1\psi_2\rangle$. The next two excited states are also triplet states, originating from the configurations $|\psi_1\psi_3\rangle$ and $|\psi_2\psi_3\rangle$, respectively. Configuration interaction mixes states of the same spin multiplicity, leading to a ground state that has contributions from several configurations ($|\psi_1\psi_1\rangle$, $|\psi_1\psi_3\rangle$, and $|\psi_2\psi_2\rangle$), as shown in Figure 7d. Strong correlation effects alter the distribution of the two electrons. A plot of the correlation function (bottom

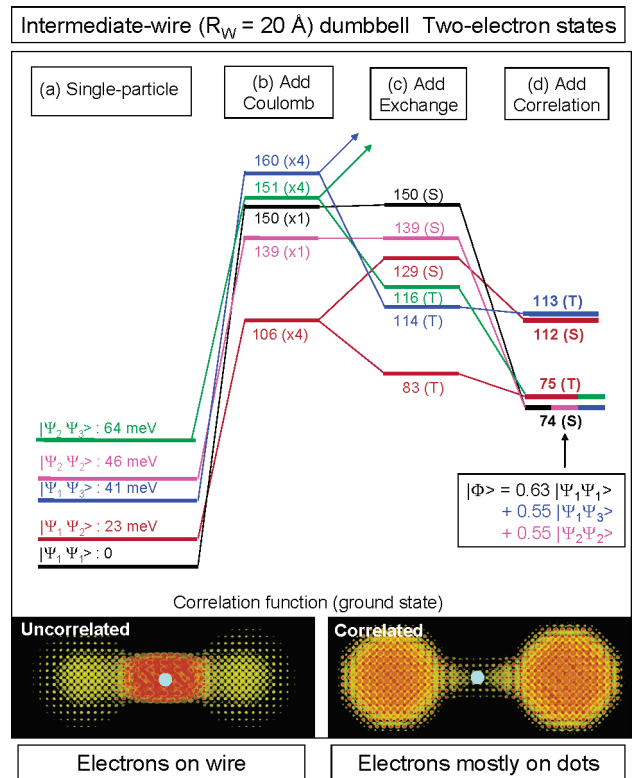


Figure 7. Energy levels (in meV) of two electrons in an intermediate-wire nano dumbbell ($R_w = 10 \text{ \AA}$). The correlation function in the uncorrelated (single-particle) and correlated (full CI) cases is shown at the bottom of the figure. The correlation function gives the probability of finding one electron in different regions of the dumbbells (yellow cloud), when the other electron is kept fixed at the center of the CdSe wire (blue circle).

of Figure 7) shows that while the two electrons are mainly localized on the wire in the uncorrelated case they are located on the dots when configuration interaction is taken into account. The degree of entanglement in this case has an intermediate value of 61%, showing a certain mixing of configurations that does not lead, however, to a purely symmetric or antisymmetric state with maximum entanglement. The next excited state originates from the $|\psi_1\psi_2\rangle$ triplet states with some admixture of $|\psi_2\psi_3\rangle$ character (Figure 7d). These 3-fold degenerate states have a degree of entanglement between 80% and 97%.

The localization of the single-particle wave functions has direct consequences on the optical properties of the nano dumbbells. As the wire becomes narrower, the CBM wave function migrates from the CdSe wire to the CdTe dots, while the VBM wave function remains localized on the CdTe dots, as shown in Figure 3. Thus, the band alignment of the dumbbell changes from type I to type II, affecting the exciton binding energy. We have calculated the exciton energies of the nano dumbbells using the configuration-interaction approach.²⁷ We have included two valence-band states and two conduction-band states in the CI expansion. The exciton binding energy is given by $E_b = E_X^0 - E_X$, where E_X^0 is the energy of the lowest electron–hole pair in the uncorrelated (single-particle) case and E_X is the energy of the exciton in the CI calculation. For a narrow CdSe wire ($R_w = 8 \text{ \AA}$) both the VBM and the CBM wave functions are localized on the

CdTe dots, resulting in a relatively large electron–hole binding energy ($E_b = 115$ meV). As the CdSe wire becomes wider, the exciton binding energy decreases to 86 meV for $R_w = 10$ Å and 59 meV for $R_w = 15$ Å.

In conclusion, we have shown that the localization of the single-particle wave functions in CdSe/CdTe nano dumbbells can be controlled by changing the radius of the CdSe wire. As the wire becomes narrower, the wire electron states are pushed higher in energy compared to the dot electron states, so the lowest electron state changes its localization from the wire to the dots. We have also demonstrated that, when the radius of the CdSe wire is small ($R_w \leq 10$ Å), strong correlation effects determine the spatial localization and the degree of entanglement of the two-electron wave functions. As previously shown,³⁶ carrier localization and wave function entanglement are not “frozen in” for a given nanostructure composition, shape, and size but can be deliberately tuned by applying an external electric field. Our methodology provides an accurate way to characterize the most important features that are currently not accessible experimentally, i.e., the degree of carrier localization and wave function entanglement. Our results illustrate how complex semiconductor nanostructures such as nano dumbbells can serve as a platform to simultaneously manipulate quantum confinement, electron–electron correlation, and wave function entanglement and can provide the basic architectural elements of nanodevices.

Acknowledgment. This work was supported by the DOE-SC-BES initiative LAB03-17, under NREL Contract No. DE-AC36-99GO10337.

References

- (1) Collins, P. G.; Avouris, P. *Sci. Am.* **2000**, 283, 62.
- (2) Huang, Y.; Duan, X.; Cui, Y.; Lauhon, L. J.; Kim, K. H.; Lieber, C. M. *Science* **2001**, 294, 1313.
- (3) Klein, D. L.; Roth, R.; Lim, A. K. L.; Alivisatos, A. P.; McEuen, P. L. *Nature* **1997**, 389, 699.
- (4) (a) Tarucha, S.; Austing, D. G.; Honda, T.; van der Hage, R. J.; Kouwenhoven, L. P. *Phys. Rev. Lett.* **1996**, 77, 3613. (b) Kouwenhoven, L. P.; Oosterkamp, T. H.; Danoesastro, M. W. S.; Eto, M.; Austing, D. G.; Honda, T.; Tarucha, S. *Science* **1997**, 278, 1788.
- (5) Warburton, R. J.; C Schaflein, Haft, D.; Bickel, F.; Lorke, A.; Karrai, K.; Garcia, J. M.; Schoenfeld, W.; Patroff, P. M. *Nature* **2000**, 405, 926.
- (6) Reuter, D.; Kailuweit, P.; Wieck, A. D.; Zeitler, U.; Wibbelhoff, O.; Meier, C.; Lorke, A.; Maan, J. C. *Phys. Rev. Lett.* **2005**, 94, 026808.
- (7) *International Technology Road Map for Semiconductors*. <http://public.itrs.net>.
- (8) Loss, D.; DiVincenzo, D. P. *Phys. Rev. A* **1998**, 57, 120.
- (9) Bimberg, D.; Ledentsov, N. N.; Grundmann, M. *Quantum Dot Heterostructures*; Wiley: New York, 1999.
- (10) Lieber, C. M. *MRS Bull.* **2003**, 28, 486.
- (11) Bastard, G. *Wave Mechanics Applied to Semiconductor Heterostructures*; Les Editions de Physique: Les Ulis, France, 1988.
- (12) (a) Yannouleas, C.; Landman, U. *Phys. Rev. Lett.* **1999**, 82, 5325. (b) Troiani, F.; Hohenester, H.; Molinari, E. *Phys. Rev. B* **2002**, 65, 161301. (c) Bester, G.; Shumway, J.; Zunger, A. *Phys. Rev. Lett.* **2004**, 93, 047401.
- (13) Remacle, F.; Levine, R. D. *J. Phys. Chem. B* **2001**, 105, 2153.
- (14) Mokari, T.; Rothenberg, E.; Popov, I.; Costi, R.; Banin, U. *Science* **2004**, 304, 1787.
- (15) Bakkers, E. P. A. M.; Hens, Z.; Zunger, A.; Franceschetti, A.; Kouwenhoven, L. P.; Gurevich, L.; Vanmaekelbergh, D. *Nano Lett.* **2001**, 1, 55.
- (16) Brus, L. E. *J. Chem. Phys.* **1983**, 79, 5566.
- (17) Al. Efros, L.; Rosen, M. *Annu. Rev. Mater. Sci.* **2000**, 30, 475.
- (18) (a) Pederiva, F.; Umrigar, C. J.; Lipparini, E. *Phys. Rev. B* **2000**, 62, 8120. (b) Shumway, J.; Fonseca, L. R. C.; Leburton, J. P.; Martin, R. M.; Ceperley, D. M. *Physica E* **2000**, 8, 260.
- (19) Stier, O.; Grundmann, M.; Bimberg, D. *Phys. Rev. B* **1999**, 59, 5688.
- (20) Hawrylak, P.; Korkusinski, M. *Top. Appl. Phys.* **2003**, 90, 25.
- (21) (a) Jiang, H.; Singh, J. *Appl. Phys. Lett.* **1997**, 71, 3239. (b) Fu, H.; Wang, L. W.; Zunger, A. *Phys. Rev. B* **1998**, 57, 9971.
- (22) Zunger, A. *Phys. Status Solidi A* **2002**, 190, 467.
- (23) Bester, G.; Shumway, J.; Zunger, A. *Phys. Rev. Lett.* **2004**, 93, 047401.
- (24) Delerue, C.; Lannoo, M.; Allan, G. *Phys. Status Solidi B* **2001**, 227, 115.
- (25) Wang, L. W.; Zunger, A. *J. Chem. Phys.* **1994**, 100, 2394.
- (26) Lee, S.; Kim, J.; Jonsson, L.; Wilkins, J. W.; Bryant, G. W.; Klimeck, G. *Phys. Rev. B* **2002**, 66, 235307.
- (27) Franceschetti, A.; Fu, H.; Wang, L. W.; Zunger, A. *Phys. Rev. B* **1999**, 60, 1819.
- (28) Rohlfing, M.; Louie, S. G. *Phys. Rev. Lett.* **1998**, 80, 3320.
- (29) Williamson, A. J.; Grossman, J.; Hoods, R. Q.; Puzder, A.; Galli, G. *Phys. Rev. Lett.* **2002**, 89, 196803.
- (30) Wang, L. W. *Phys. Rev. Lett.* **2002**, 88, 256402.
- (31) Wang, L. W.; Li, J. *Phys. Rev. B* **2004**, 69, 153302.
- (32) Wei, S. H.; Zunger, A. *Appl. Phys. Lett.* **1998**, 72, 2011.
- (33) Delerue, C.; Allan, G.; Lannoo, M. *Phys. Rev. B* **2003**, 68, 115411.
- (34) Cartoixa, X.; Wang, L. W. *Phys. Rev. Lett.* **2005**, 94, 236804.
- (35) He, L.; Bester, G.; Zunger, A. *Phys. Rev. B* **2005**, 72, 195307.
- (36) Bester, G.; Zunger, A. *Phys. Rev. B* **2005**, 72, 165334.

NL052511V